
Engineering Physics (B. Eng.)

Bachelor Thesis

# Fiber Induced Optical Phase Noise Mitigation

*Author:*
Babette von Boetticher

*Supervisors:*
Prof. Dr.-Ing. Philipp Huke
Dr. Matthieu Gosselin

Oldenburg, 12.11.2022

**Abstract**

The aim of this thesis is to experimentally investigate how environmental acoustic and seismic noise is induced in optical fibers as optical phase noise and investigate different approaches to mitigating the noise. At first, the theoretical concepts of optical phase noise are explained and the beating signal, which will be recorded, is mathematically derived. Next, the experimental setup, a heterodyne interferometer, is assembled such that the reference arm is acoustically and seismically well isolated from the test arm. Subsequently, optical components are tested on their sensitivity to the injected environmental noise in terms of the induced optical phase noise. The assumption that longer fiber length and thinner fiber jackets negatively influence the induced optical phase noise under acoustic and seismic noise is experimentally confirmed. Finally, three manners of mitigating the optical phase noise induction are attempted. As a result, taping the fiber to the bench is unfavorable for the fiber's sensitivity. Isolating the fiber in an aluminum box filled with a silicone sealant can improve the sensitivity at the main resonance frequency to seismic noise. Suspending the box containing the fiber seems the most useful, mostly to mitigate the induced phase noise due to seismic environmental noise, and leads to better results, hence a lower optical phase noise, the higher the suspended mass is.

# Contents

# List of Figures

# List of Tables

# 1 Introduction

Since the first detection of a gravitational wave, trembles in the space-time continuum, on September $14^{\text{th}}$, 2015 the detectors have undergone multiple rounds of modifications to increase their sensitivity and hence look "further" into space. Gravitational wave detection is based on a large laser interferometer. The main principle of the detection of gravitational waves is interference, which is based on the length change and hence phase shift between the light of the two interferometer arms. Since gravitational waves produce only tiny length changes (order of magnitude $10^{-21}$), their detection is extremely sensitive to noise including all variations in laser light characteristics. In order to increase the sensitivity of a gravitational wave detector, it is one of the major goals to minimize the inherent phase noise of the laser. When using optical fibers, as largely done in the injection lab of the interferometer, a problem that arises is the coupling of environmental noise into the fiber as optical phase noise. Consequently, the aim of this thesis is to experimentally investigate how environmental acoustic and seismic noise is induced in optical fibers as optical phase noise and to attempt different ways of mitigating the noise. The work presented in this thesis was executed at the European Gravitational observatory (EGO) which is responsible for the functioning and maintenance of the Virgo gravitational wave detector in Cascina, Italy.

In Chapter 2, the basic theoretical concepts of optical phase noise and its importance in gravitational wave detection are explained. Additionally, the beating signal representing the optical phase noise measured using a specific experimental setup is mathematically described. At last, the working principles of optical fibers and the acousto-optic modulator are illustrated. In Chapter 3, the experimental setup of a heterodyne interferometer is described in more detail and is set up step by step in order to enable measuring the beating signal produced by the induced optical phase noise through injected acoustic or seismic noise. The utilized optical fibers and fiber connectors will be named and the acoustic and seismic noise spectra which are going to be injected into the test arm are shown. To increase the isolation of the reference arm of the interferometer from the injected environmental noise, a box containing the reference arm is installed and characterized. In Chapter 4, the performed experiments are described and analyzed. First, the effect of acoustic and seismic noise injection, respectively, on various optical fibers with different lengths or jackets as well as fiber connectors are investigated. Next, three ways of mitigating the optical phase noise induced by environmental noise are attempted, namely the taping of the fiber under test to the bench, isolating the fiber in an aluminum box, and suspending the fiber in the box using a spring. Chapter 5 finally summarizes the experimentally obtained results and presents options for further investigations.

# 2 Theory

This chapter will introduce all theoretical concepts needed for this thesis. In Chapter 2.1, the concept of optical phase noise is explained as well as its importance in gravitational wave detection. In Chapter 2.2, the theory behind the experimental setup is discussed in more depth and the mathematical derivation of the beating signal representing the optical phase noise, which will be recorded in the experiments, is given. Finally, the theoretical concepts of some key components, namely optical fibers and the acousto-optic modulator (AOM), which are utilized in the experiments are explained in Chapter 2.3.

## 2.1 Optical Phase Noise

This chapter explains the concept of optical phase noise and discusses its relevance in gravitational wave detection.

### 2.1.1 General

Optical phase noise refers to the random fluctuations in the optical phase of the light from a monochromatic laser [1]. Phase noise directly relates to frequency noise since the instantaneous frequency of a laser can also be represented as the temporal derivative of the phase [2]. Consequently, phase noise produces a finite linewidth of the laser output. While phase noise describes the spectral deviations in the frequency domain, the temporal deviations from the period in the time domain are called jitter. Both are directly related to each other.

The optical phase noise is mainly caused by quantum noise or other technical noise inside the gain medium and resonator mirrors. Phase noise can also be introduced through optical media on the laser path, e.g. due to mirror vibrations. In this thesis, however, the optical phase noise induced in optical fibers through environmental acoustic and seismic noise will be analyzed and mitigated. The injected acoustic and seismic noise cause vibrations of the fiber under test (FUT) which lead to minor changes in the laser's optical path length. These oscillations in optical path length are consequently transferred as optical phase noise of the laser and can be measured with a suitable setup.

### 2.1.2 Importance in Gravitational Wave Detection

Before discussing the significance of optical phase noise in gravitational wave detection, the concept of gravitational waves itself must be explained first. Gravitational waves are disturbances or trembles of the space-time continuum, which propagate at the speed of light and transport information about the physics of their astrophysical and cosmological sources [3]. This allows the gain of information about sources which do not emit electro-

magnetic waves or expands the available information about those that do.

Gravitational waves are basically detected by using a large modified Michelson interferometer. When a gravitational wave strikes the interferometer, the arms experience minimal temporal length fluctuations, altering the path length of the light in the interferometer arms by a length $\Delta L$ [4]. The relative length changes of the detector arms caused by gravitational waves are in the order of magnitude of $10^{-21}$ and thus extremely small. The length variation modifies the phase difference $\Delta\phi = 2\pi\Delta L/\lambda$ (with $\lambda$ the wavelength of the laser) between the two partial light beams of the interferometer arms at the beam splitter. As a result, an optical signal which is proportional to the gravitational wave strain is transmitted to the final photo detector. Ideally, the interferometer works with the "dark fringe", meaning that it is set to have zero intensity at the detector in its unperturbed state [3]. This way, changes in the intensity of the interference pattern of the light at the detector can be detected most easily. A gravitational wave passing the interferometer causes the stretch of one arm and compression of the other at the frequency of the incident gravitational wave. As a consequence, the light returns at a slightly different time, and hence phase, from each arm and the two light beams do not completely cancel anymore (to form the dark fringe). The process is then reversed in an oscillating manner. The path difference of the arms is a measure of the intensity of the space-time fluctuations due to the incident gravitational wave. In the interferometer, space-time fluctuations are converted into intensity fluctuations of the laser light due to its phase difference, which makes the gravitational wave detectable and measurable through intensity measurements using a photo detector.

The main challenge in gravitational wave detection using the laser interferometer lies in making the detector sensitive to the incredibly tiny distortions of space coming from a gravitational wave, while at the same time suppressing various types of background noise [5]. The interferometer is disturbed by different kinds of frequency-dependent noise simultaneously. This includes thermal noise, acoustics noise, seismic noise, quantum noise, gravitational noise, photon shot noise, scattered-light noise etc, to name only a few. The sensitivity of gravitational wave detection can be compared to the measurement of sea level rise when pouring a glass of water into the ocean. To enable the detection of a gravitational wave, an important factor to be considered is the utilized laser light. The laser needs to be highly stable in all its characteristics including its monochromatic frequency, linear polarization, high power, and all characteristics related to these.

In summary, a modified Michelson interferometer, which works by detecting the length and thus phase change between the two detector arms at the photo detector, is used. However, the relative change in arm length ($\Delta L/L$) is only $10^{-21}$ and is highly disturbed

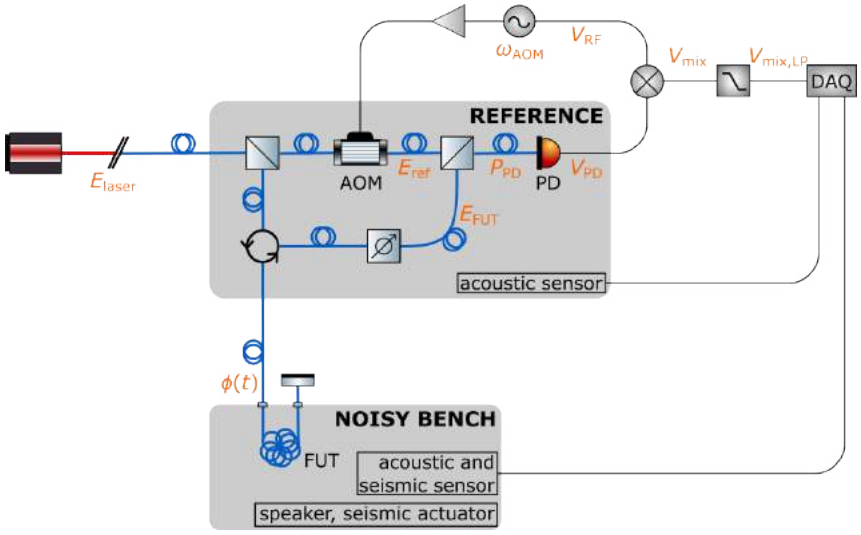


Fig. 2.1: Sketch of the experimental setup to measure the optical phase noise induced due to environmental noise, including variables for the mathematical derivation

by numerous types of noise [5]. Therefor, the phase noise which is induced in optical fibers caused by acoustic or seismic environmental noise directly influences the sensitivity of the detection of gravitational waves. Consequently, analyzing and mitigating this optical phase noise is going to be the task and topic of this thesis.

## 2.2 Mathematical Derivation of the Beating Signal

The following mathematical derivation of the beating signal, i.e. the phase noise, was derived with Matthieu Gosselin [6, 7] and is based on Chapter 4.4.5 of his PhD thesis [8].

Employing a setup as shown in Figure 2.1, the optical phase noise introduced by environmental noise, here acoustic and seismic noise, can be measured. Essentially, the setup is based on a self-heterodyne interferometer, where the frequency of the laser light in the reference arm is modulated using an acousto-optic modulator (AOM) and the light which passes the fiber under test (FUT) is subject to environmental noise injection, here acoustic and seismic noise. The light from the reference and FUT arm is subsequently recombined and superposed, then detected with a photodiode, and demodulated with the same frequency as the AOM. A low-pass filter then passes only the relevant DC part, which is recorded and read through the data acquisition device (DAQ).

The laser light has an initial electric field of

$$E_{\text{laser}} = A_0 \cdot \mathrm{e}^{i(\omega_0 t + \varphi_0)}, \tag{1}$$

where $A_0$ is the amplitude fluctuating over time with the laser frequency $\omega_0$ and $\varphi_0$ the random initial phase. In reality, fluctuations can also arise independently, however, these

will be neglected in the following derivation. This light is divided using a beam splitter, where one part is going to the FUT arm and the the other part to the reference arm.

The frequency of the light passing the reference arm is modulated by the AOM at the frequency $\omega_{\mathrm{AOM}}$. Consequently, the electric field of the modulated reference beam can be described as follows

$$E_{\mathrm{ref}} = A_1 \cdot \mathrm{e}^{i((\omega_0+\omega_{\mathrm{AOM}})t+\varphi_0+\varphi_1)}, \tag{2}$$

with $A_1$ the amplitude, $\omega_{AOM}$ the modulation frequency, and $\varphi_1$ the additional constant phase shift due to the optical path difference. As a result, the light of the reference arm oscillates at a frequency of $\omega_0 + \omega_{\mathrm{AOM}}$.

The light in the FUT arm generally maintains its frequency when undisturbed. However, due to the injected environmental noise an additional time-dependent phase noise $\phi(t)$ is introduced. This phase noise is the key element to be investigated throughout the experiments in this thesis. As a consequence, the equation for the electric field of the light in the FUT arm is

$$E_{\mathrm{FUT}} = A_2 \cdot \mathrm{e}^{i(\omega_0 t+\varphi_0+\varphi_2+\phi(t))}, \tag{3}$$

with $A_2$ the amplitude, $\varphi_2$ the additional constant phase shift due to the optical path difference, and $\phi(t)$ the optical phase noise. Since $\varphi_0$, $\varphi_1$, and $\varphi_2$ fluctuate significantly more slowly than the induced optical phase noise $\phi(t)$ which is studied, they can be considered as constant and thus will be neglected in the derivation. Eq. 2 and 3 subsequently become

$$E_{\mathrm{ref}} = A_1 \cdot \mathrm{e}^{i(\omega_0+\omega_{\mathrm{AOM}})t} \tag{4}$$

$$E_{\mathrm{FUT}} = A_2 \cdot \mathrm{e}^{i(\omega_0 t+\phi(t))}. \tag{5}$$

The power signal of the light from the two superposed arms which is detected at the photodiode is given by

$$\begin{aligned} P_{\mathrm{PD}} &= (E_{\mathrm{ref}} + E_{\mathrm{FUT}})(E_{\mathrm{ref}} + E_{\mathrm{FUT}})^* \\ &= A_1^2 + A_2^2 + E_{\mathrm{ref}}E_{\mathrm{FUT}}^* + E_{\mathrm{ref}}^* E_{\mathrm{FUT}}, \end{aligned} \tag{6}$$

where

$$\begin{aligned} E_{\mathrm{ref}}E_{\mathrm{FUT}}^* &= A_1 A_2 \cdot \mathrm{e}^{i(\omega_0+\omega_{\mathrm{AOM}})t} \cdot \mathrm{e}^{-i(\omega_0 t+\phi(t))} \\ &= A_1 A_2 \cdot \mathrm{e}^{i(\omega_{\mathrm{AOM}} t-\phi(t))} \end{aligned} \tag{7}$$

and

$$\begin{aligned} E_{\mathrm{ref}}^* E_{\mathrm{FUT}} &= A_1 A_2 \cdot \mathrm{e}^{-i(\omega_0+\omega_{\mathrm{AOM}})t} \cdot \mathrm{e}^{i(\omega_0 t+\phi(t))} \\ &= A_1 A_2 \cdot \mathrm{e}^{-i(\omega_{\mathrm{AOM}} t-\phi(t))} \end{aligned} \tag{8}$$

yield

$$\begin{aligned} E_{\mathrm{ref}}E^*_{\mathrm{FUT}} + E^*_{\mathrm{ref}}E_{\mathrm{FUT}} &= A_1A_2 \cdot \left(\mathrm{e}^{i(\omega_{\mathrm{AOM}}t-\phi(t))} + \mathrm{e}^{-i(\omega_{\mathrm{AOM}}t-\phi(t))}\right) \\ &= 2A_1A_2 \cdot \cos(\omega_{\mathrm{AOM}}t - \phi(t)) \end{aligned} \tag{9}$$

and therefore results in

$$P_{\mathrm{PD}} = A_1^2 + A_2^2 + 2A_1A_2 \cdot \cos(\omega_{\mathrm{AOM}}t - \phi(t)). \tag{10}$$

This resulting power $P_{\mathrm{PD}}$ can be split up in a constant DC part

$$P_{\mathrm{DC}} = A_1^2 + A_2^2 \tag{11}$$

and an AC part

$$P_{\mathrm{AC}} = 2A_1A_2 \cdot \cos(\omega_{\mathrm{AOM}}t - \phi(t)) \tag{12}$$

oscillating with the modulation frequency $\omega_{\mathrm{AOM}}$ and containing the time-dependent optical phase noise $\phi(t)$, such that

$$P_{\mathrm{PD}} = P_{\mathrm{DC}} + P_{\mathrm{AC}}. \tag{13}$$

The photodiode then converts the power signal into a voltage signal with a specific responsivity or gain factor $G$ (with unit V/W). Hence, the resulting voltage is given by

$$\begin{aligned} V_{\mathrm{PD}} &= G \cdot P_{\mathrm{PD}} \\ &= GP_{\mathrm{DC}} + 2GA_1A_2 \cdot \cos(\omega_{\mathrm{AOM}}t - \phi(t)). \end{aligned} \tag{14}$$

The voltage signal of the photodiode $V_{\mathrm{PD}}$ is subsequently demodulated with a reference voltage signal $V_{\mathrm{RF}}$ produced by the RF function generator with the same frequency as previously used for the modulation with the AOM. The resulting signal after the demodulation can be described as follows

$$V_{\mathrm{mix}} = V_{\mathrm{PD}} \cdot V_{\mathrm{RF}} \tag{15}$$

with

$$V_{\mathrm{RF}} = A_{\mathrm{RF}} \cdot \cos(\omega_{\mathrm{AOM}}t), \tag{16}$$

where $A_{\mathrm{RF}}$ is the amplitude of the voltage signal. From Eq. 14-16 follows

$$\begin{aligned} V_{\mathrm{mix}} = {} & GP_{\mathrm{DC}}A_{\mathrm{RF}} \cdot \cos(\omega_{\mathrm{AOM}}t) \\ & + 2GA_1A_2A_{\mathrm{RF}} \cdot \cos(\omega_{\mathrm{AOM}}t - \phi(t)) \cdot \cos(\omega_{\mathrm{AOM}}t). \end{aligned} \tag{17}$$

Applying the following trigonometric identity

$$\cos(x)\cos(y) = \frac{\cos(x-y) + \cos(x+y)}{2} \tag{18}$$

results in

$$\begin{aligned} V_{\text{mix}} = & GP_{\text{DC}}A_{\text{RF}} \cdot \cos(\omega_{\text{AOM}}t) \\ & + GA_1A_2A_{\text{RF}} \cdot [\cos(\phi(t)) + \cos(2\omega_{\text{AOM}}t - \phi(t))] \,. \end{aligned} \tag{19}$$

We then define

$$V_{\text{mix}} = V_{\text{mix,DC}} + V_{\text{mix},\omega_{\text{AOM}}} + V_{\text{mix},\omega_{2\text{AOM}}}, \tag{20}$$

with

$$V_{\text{mix,DC}} = GA_1A_2A_{\text{RF}} \cdot \cos(\phi(t)) \tag{21}$$

$$V_{\text{mix},\omega_{\text{AOM}}} = GP_{\text{DC}}A_{\text{RF}} \cdot \cos(\omega_{\text{AOM}}t) \tag{22}$$

$$V_{\text{mix},\omega_{2\text{AOM}}} = GA_1A_2A_{\text{RF}} \cdot \cos(2\omega_{\text{AOM}}t - \phi(t)). \tag{23}$$

$V_{\text{mix,DC}}$ is the only part of $V_{\text{mix}}$ which directly depends on the phase noise $\phi(t)$ which is to be analyzed, while all remaining variables are constants, and it oscillates at low frequencies (connected to the low frequency injected environmental noise). Since $\omega_{\text{AOM}}$ can be adjusted to a high frequency, a low-pass filter can be applied to isolate $V_{\text{mix,DC}}$ from $V_{\text{mix},\omega_{\text{AOM}}}$ and $V_{\text{mix},\omega_{2\text{AOM}}}$. Behind the low-pass filter, the obtained voltage signal is

$$V_{\text{mix,LP}} = V_{\text{mix,DC}} \tag{24}$$

$$= GA_1A_2A_{\text{RF}} \cdot \cos(\phi(t)) \tag{25}$$

$$= K \cdot \cos(\phi(t)) \tag{26}$$

with the constant $K = GA_1A_2A_{\text{RF}}$. The signal of $V_{\text{mix,LP}}$ is the so-called beating signal (in time domain). By computing its fast fourier transform (FFT), the amplitude spectral density (short "amplitude") of the beating signal and thus of the frequencies contained in the induced optical phase noise can be analyzed.

## 2.3 Working Principle of Utilized Components

In the following, the working principles of two fundamental components utilized in the experiments are explained. In Chapter 2.3.1, the basic concepts of optical fibers as well as some of their more particular designs are introduced. Chapter 2.3.2 explains the operating principle of an acousto-optic modulator.

### 2.3.1 Optical Fibers

Optical fibers are utilized to easily transport an optical signal to remote places with low losses in optical power and low beam divergence [8, 9]. Generally, optical fibers are made of glass and their working principle is based on the phenomenon of total internal reflection at the interface between the fiber core and its surrounding cladding. Therefor, the total

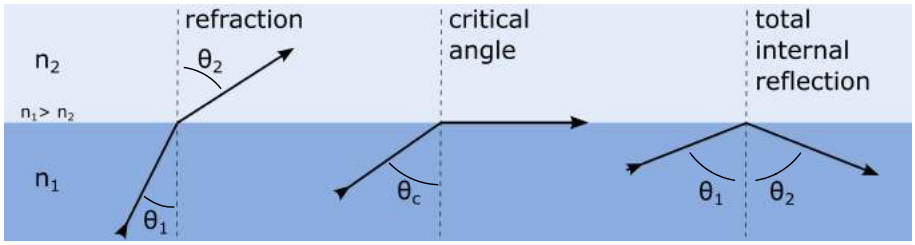


Fig. 2.2: Behavior of light beam at the interface between two media with refractive indices $n_1$ and $n_2$, where $n_1 > n_2$

internal reflection resulting from Snell's law enables the guiding of light in an optical fiber. Snell's law, as stated in Eq. 27, describes the behavior of a light beam at the interface between two media with refractive indices $n_1$ and $n_2$.

$$n_1 \cdot \sin(\theta_1) = n_2 \cdot \sin(\theta_2) \tag{27}$$

Consequently, a light beam incident at the interface at an angle larger than the critical angle $\theta_c = \arcsin(n_2/n_1)$ is totally internally reflected such that $\theta_1 = \theta_2$. Figure 2.2 gives a visualization of the three different cases occurring for $n_1 > n_2$ depending on the angle of incidence.

Figure 2.3 shows a simple sketch of an optical fiber's the basic structure. The core of high refractive index contains the optical signal and is surrounded by the low-index cladding [10]. Total internal reflection subsequently occurs at the core-cladding interface and confines the light beam to the core. The core-cladding structure made of glass is protected from external damage by a coating, strength member and outer jacket.

The most simple design of an optical fiber consisting of a cylindrical core with high refractive index surrounded by a low-index cladding, as described so far, is called a step-index fiber due to its abrupt change in refractive index [9]. A sketch of the step-index fiber

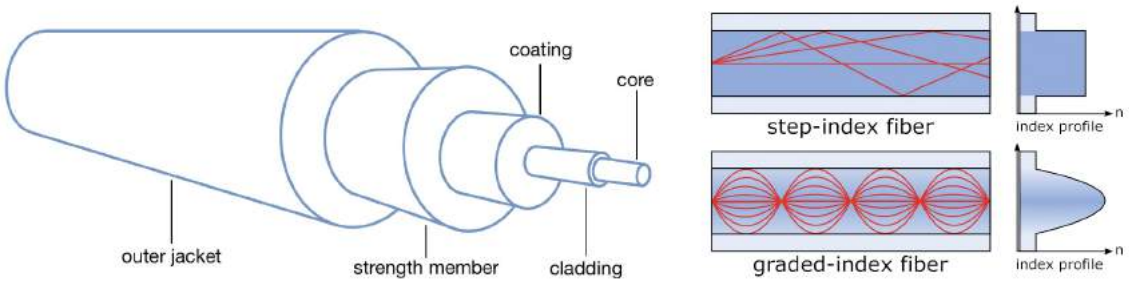


Fig. 2.3: Sketches showing the working principle of optical fibers: basic structure of optical fiber (left); beam propagation and index profile in a step-index and graded-index fiber (right)

is shown in Figure 2.3. At the core-cladding interface, the light beam experiences total internal reflection for angles larger than the critical angle $\theta_c$ throughout the entire fiber length, subsequently causing the light to stay confined to the fiber core.

In a graded-index fiber, the refractive index is not constant but gradually decreases from its maximum value at the center of the core to its minimum value at the core-cladding interface [9]. A sketch of the graded-index fiber is shown in Figure 2.3. As a result of the changes in refractive index the beam velocity changes along the fiber radius. A beam along the fiber axis follows the shortest path but propagates at the lowest speed since it passes in the material with the highest refractive index. Consequently, the beam paths no longer follow a straight oblique line but curve with the index gradient, following a sinusoidal shape instead.

A common issue in optical fibers is the broadening of individual optical pulses due to fiber dispersion when propagating through a fiber [9]. This effect occurs most strongly in multi-mode fibers as different speeds are associated with different fiber modes. Consequently, it is beneficial to use single-mode fibers instead. Single-mode fibers only support the fundamental mode of a fiber which propagates along the fiber axis. The fiber is designed in a way that for a specific cut-off wavelength all higher-order fiber modes are cut-off.

When working with optical fibers, it is also often important to maintain the polarization state of the light at the fiber output. However, every little default in the fiber structure causes small birefringence which in turn depolarizes the light and hence causes a random polarization state at the fiber output [8]. This problem can be solved by using polarization-maintaining fibers which are specially designed to maintain a stable state of polarization at the fiber output. By intentionally introducing artificial high uniform stress and thus birefringence, polarization stability can be provided [8, 10]. The introduced stress consequently produces a fast and a slow main axis with the fast axis having a lower refractive index than the slow axis. The two perpendicular main axes are constant and linear along the fiber, so that a linearly polarized light beam which is aligned to one of the main axes propagates through the fiber without undesirable changes in its polarization state and hence remains polarized on the same axis at the fiber output. It has to be noted that in case the linearly polarized light is not launched into the fiber precisely on one main axis, the polarization is split into a part on each main axis, causing a phase delay between the two parts at the fiber output. Figure 2.4 displays three possible configurations to introduce birefringence in an optical fiber, making it polarization-maintaining, namely the PANDA, bow tie and elliptical cladding designs. Although the polarization is quite well maintained, defects can still induce additional undesired birefringence which in turn causes a small amount of depolarization.

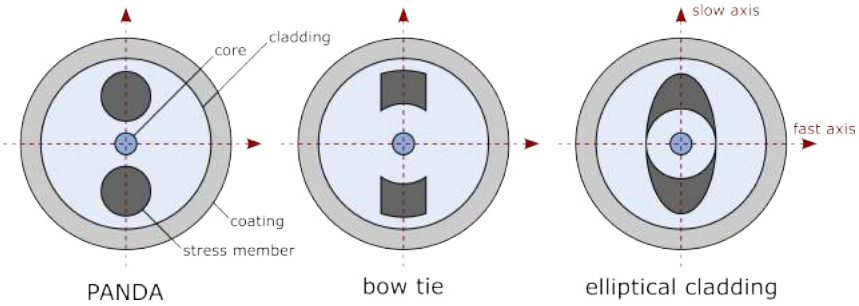


Fig. 2.4: Sketch of cross-sections for different polarization-maintaining fiber designs, where the areas of gray color are additional stress elements in the cladding

### 2.3.2 Acousto-Optic Modulator

Acousto-optic modulators (AOM) are based on the photo-elastic effect, which describes the changes in optical properties of the acousto-optic crystal due to the mechanical strain, here produced by an acoustic signal [11]. A piezoelectric transducer receives a signal from an RF function generator and consequently excites a sound wave generating a periodically oscillating mechanical strain wave in the crystal. The oscillating strain wave results in a periodically changing index of refraction and hence periodically changing optical properties of the crystal. Due to the photo-elastic effect, a refractive index grating traveling at the speed of sound is created at which the light passing the AOM is diffracted (Bragg diffraction). As a consequence, the optical frequency, propagation direction, and intensity of the light are modified. In the following experiments, benefit will be taken of the frequency-modulation of the laser light. The utilized AOM is built so that the first order diffracted beam is injected into the output fiber and the optical frequency will be shifted by the frequency $\omega_{\mathrm{AOM}}$ of the sound wave in the AOM. Figure 2.5 schematically visualizes the working principle of an AOM.

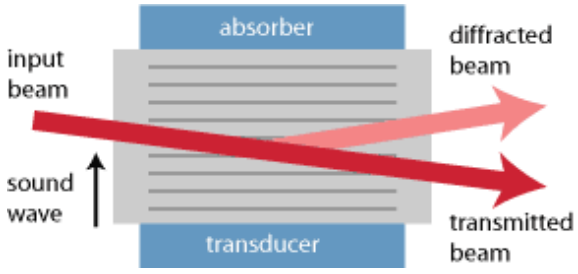


Fig. 2.5: Schematic setup of an acousto-optic modulator [12]

# 3 Experimental Setup

The setup of the experiment to detect and measure the optical phase noise induced in optical fibers through injected environmental noise will be set up as already briefly described in Chapter 2.2. This chapter covers the more practical part of the setup including the process of setting up the experiment, parameters chosen for the individual components, as well as characterizations of the injected acoustic and seismic noise and the isolation using the reference box.

## 3.1 General Setup

The theoretical setup as shown in Figure 2.1 needs to be extended by its working parameters. For this purpose, the experimental setup has to be assembled step by step.

At first, the electronics part of the reference arm, i.e. the RF amplifier and AOM, is characterized. For a start, the gain of the RF amplifier is determined measuring the output peak-to-peak voltage $V_{\mathrm{pp}}$ with an oscilloscope depending on the frequency $f$ and the power $P_{\mathrm{in}}$ of the input signal, respectively, and from that finding the gain $G$. A simple schematic of the setup is shown in Figure 3.1. From the measured output voltage $V_{\mathrm{pp}}$ the gain of the amplifier is found as follows

$$G_{\mathrm{dB}} = P_{\mathrm{out(dBm)}} - P_{\mathrm{in}} \tag{28}$$

$$= 10 \cdot \log\left(\frac{P_{\mathrm{out(W)}}}{1\ \mathrm{mW}}\right) - P_{\mathrm{in}} \tag{29}$$

$$= 10 \cdot \log\left(\frac{V_{\mathrm{pp}}^2}{8R \cdot 1\ \mathrm{mW}}\right) - P_{\mathrm{in}}, \tag{30}$$

with $R = 50\,\Omega$ the input impedance of the oscilloscope. Table 3.1 shows the results for a constant input power of $P_{\mathrm{in}} = -10$ dBm and varying the frequency $f$ between 60 MHz and 100 MHz. The resulting average gain of the amplifier for the measurement is 40.59 dB. Table 3.2 shows the results for a constant frequency of $f = 80$ MHz and varying the input power $P_{\mathrm{in}}$ between $-20$ dBm and $-8$ dBm. The resulting average gain of the amplifier for the measurement is 40.73 dB. Generally, it is found that the amplifier is not considerably sensitive to changes in frequency or input power and its functioning will consequently not interfere with the measurement.

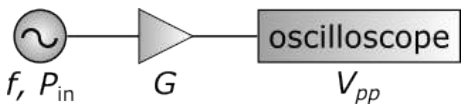


Fig. 3.1: Schematic of setup to characterize gain $G$ of RF amplifier depending on frequency $f$ and input power $P_{\mathrm{in}}$ by measuring the output peak-to-peak voltage $V_{\mathrm{pp}}$

Table 3.1: Measured peak-to-peak voltage $V_{pp}$ at the output of the RF amplifier depending on the frequency $f$ with a constant input power $P_{in} = -10$ dBm

| $f$ [MHz] | $V_{pp}$ [V] | $G$ [dB] |
|---|---|---|
| 60 | 20.8 | 40.34 |
| 70 | 22.0 | 40.83 |
| 75 | 21.9 | 40.79 |
| 80 | 22.0 | 40.83 |
| 85 | 21.5 | 40.63 |
| 90 | 21.1 | 40.47 |
| 100 | 20.6 | 40.26 |

Table 3.2: Measured peak-to-peak voltage $V_{pp}$ at the output of the RF amplifier depending on the input power $P_{in}$ with a constant frequency $f = 80$ MHz

| $P_{in}$ [dBm] | $V_{pp}$ [V] | $G$ [dB] |
|---|---|---|
| -20 | 6.88 | 40.73 |
| -18 | 8.80 | 40.87 |
| -16 | 10.9 | 40.73 |
| -14 | 13.8 | 40.78 |
| -12 | 17.4 | 40.79 |
| -10 | 22.0 | 40.83 |
| - 8 | 26.4 | 40.41 |

Next, the acousto-optic modulator (AOM) is characterized to find the optimal parameters for the modulation frequency $f_{AOM}$ ($\omega_{AOM} = 2\pi f_{AOM}$) and input power $P_{in}$. The modulation will be used in the reference arm of the heterodyne interferometer. The laser utilized for the experiments has a wavelength of 1064 nm, just like the laser used in the Virgo detector itself, and is set to an initial power of approximately 50 mW throughout the experiments. A simple schematic of the setup is shown in Figure 3.2.

First, the input power is set to a constant value of $P_{in} = -10$ dBm while varying the modulation frequency $f_{AOM}$ between 10 MHz and 120 MHz. A power meter then measures the laser power at the output of the AOM, i.e. the power of the first order diffracted beam in the AOM which is injected in the output fiber. Figure 3.3a displays the measured power $P_{out}$ depending on the frequency $f_{AOM}$. The global maximum of the output power is found at a frequency of 80 MHz.

Then, the modulation frequency is fixed at $f_{AOM}$ and the input power $P_{in}$ of the RF is varied between $-40$ dBm and $-7$ dBm. The power meter then again measures the laser power $P_{out}$ at the output of the AOM. Figure 3.3b displays the measured power $P_{out}$ depending on the power $P_{in}$ of the RF. The maximum laser power is found at $P_{in} = -8$ dBm.

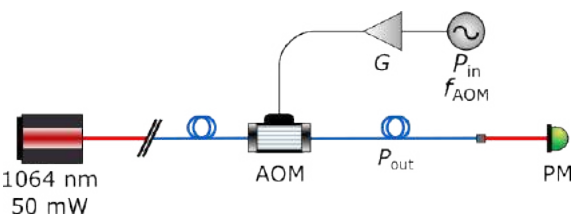


Fig. 3.2: Schematic of setup to find the best working parameters for the modulation frequency $f_{AOM}$ and input power $P_{in}$ of the AOM

Consequently, the AOM is adjusted to a modulation frequency of 80 MHz with an input power of −8 dBm.

After characterizing the AOM and determining the most suitable parameters for the modulation frequency and power, the entire setup to measure the induced optical phase noise, i.e. the beating signal, can be assembled as shown in Figure 3.4. The infrared laser with a wavelength of 1064 nm and an initial power of approximately 50 mW is coupled into an optical fiber and split by a 99:1 beam splitter into a reference arm and a test arm.

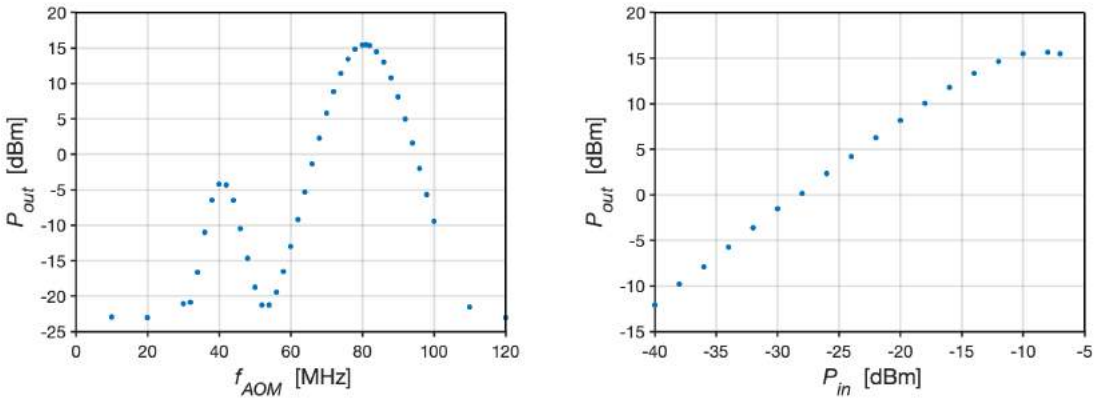


(a) constant $P_{\text{in}} = -10$ dBm (b) constant $f_{\text{AOM}} = 80$ MHz

Fig. 3.3: Laser power $P_{\text{out}}$ at output of AOM (a) depending on the modulation frequency $f_{\text{AOM}}$ and (b) depending on the RF input power $P_{\text{in}}$

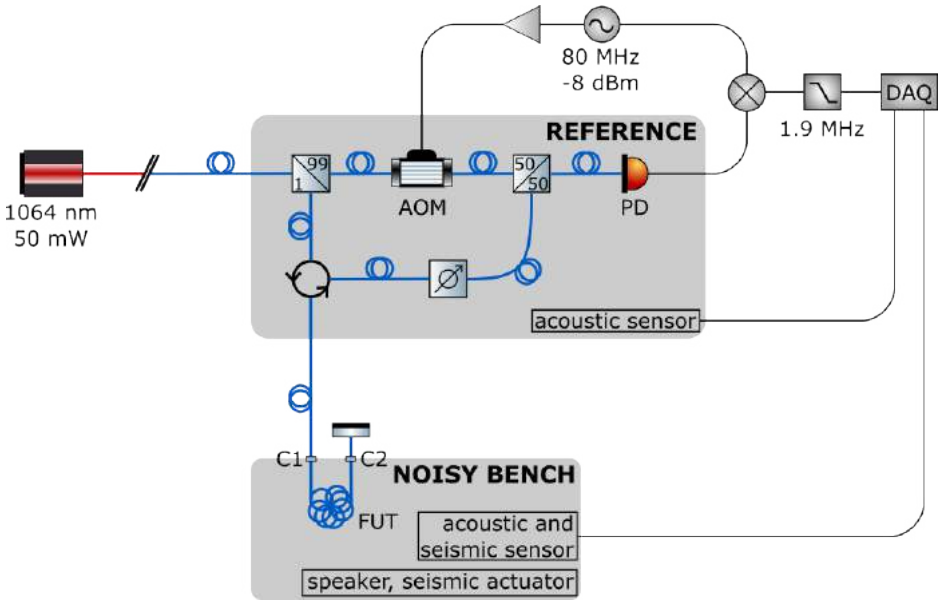


Fig. 3.4: Sketch of experimental setup to measure the optical phase noise induced by environmental noise, including selected setup parameters

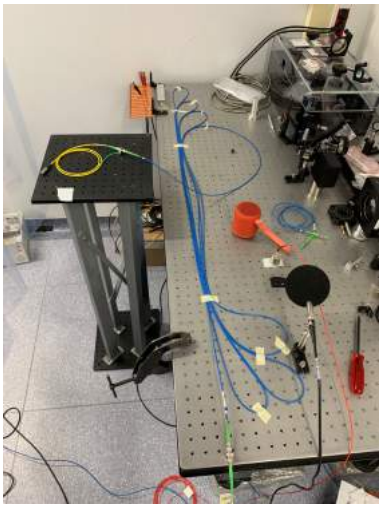

Fig. 3.5: Picture of noisy bench with FUT, speaker, seismic actuator (clamped below bench), acoustic and seismic sensor as well as separate table with fiber mirror

The laser light in the reference arm is modulated by the AOM with a frequency of 80 MHz as previously described. In the test arm, a fiber optic circulator forwards the light through a long connecting fiber into the fiber under test (FUT), which is placed on another bench, the "noisy bench", where the acoustic and seismic noise is injected. A picture of the noisy bench is shown in Figure 3.5. A fiber mirror then reflects the light back to the fiber optic circulator, where the light is guided through another fiber passing an adjustable attenuator (which is installed to guarantee a constant power at the photodiode for any FUT). The light from the reference arm and test arm is then combined via a 50:50 beam splitter (coupler in this case) and the superposed signal is finally detected by the photodiode. The final power at the photodiode is approximately 6 mW. The voltage forwarded by the photodiode is demodulated with a frequency of 80 MHz (same as $f_{\mathrm{AOM}}$) at -8 dBm. After mixing, the low pass filter with a cutoff frequency of 1.9 MHz eliminates the high-frequency parts of the signal, so that only the low-frequency beating is passed on (see Eq. 26). Ultimately, the beating signal is read and recorded by the DAQ. Additionally, an acoustic and seismic sensor ($\mathrm{AC_{FUT}}$ and $\mathrm{SEIS_{FUT}}$) are placed on the noisy bench as well as an acoustic sensor at the reference ($\mathrm{AC_{ref}}$). These three signals are passed to and read by the DAQ, as well.

As previously mentioned, the beating signal, the acoustic and seismic noise at the FUT, and the acoustic noise at the reference are all recorded via the DAQ. Using *DataDisplay* through the *ThinLinc* software, the data can be read. The FFTs of the signals are all sampled at 20 kHz, hence detecting frequencies of up to 10 kHz according to the Nyquist-Shannon sampling theorem. The number of FFTs used for averaging is set to ten throughout all measurements. Subsequently, the recorded data is saved and used for further evaluation or plotting, which is here performed with *Matlab*.

## 3.2 Utilized Optical Fibers and Fiber Connectors

All fibers under test which are utilized in the experiments are single-mode, polarization-maintaining (PM) fibers with FC/APC connectors on each end. The concepts of single-mode and PM fibers were previously explained in Chapter 2.3.1. Among others, optical fibers with a Ø3 mm jacket of various lengths (1 m, 2 m, 10 m, 36 m) were utilized. These will in the following be referred to as "blue fibers" referring to the color of their jacket. Figure 3.6 displays pictures of the utilized blue fibers of all lengths.

(a) 1 m fiber [13] (b) 2 m fiber [14] (c) 10 m fiber [15] (d) 36 m fiber on spool

Fig. 3.6: Pictures of "blue fibers" with a Ø3 mm jacket installed as the FUT

Additionally, fibers with a thinner Ø900 µm jacket are analyzed regarding of their sensitivity to environmental noise. This includes a regular optical fiber of 3 m length (see Figure 3.7a) as well as a 99:1 fiber beam splitter (see Figure 3.7b). When using the beam splitter, the single output side is used as the input and the 99 % end of the double output side is used as the output, keeping the 1 % end capped. The last fiber under test is a 10 m custom-made optical fiber with a slightly different fiber jacket than the blue fiber, which will be referred to as "10 m black fiber" due to its black color (see Figure 3.7c).

(a) 3 m thin fiber, Ø900 µm jacket [16] (b) 1x2 PM beam splitter, 99:1 split, Ø900 µm jacket [17] (c) 10 m black fiber on spool

Fig. 3.7: Pictures of other, more special fibers installed as the FUT

Figures 3.8a-c show pictures of the fiber connectors used in the experimental setup. They include one polarization-maintaining (PM) connector and two different types of non-polarization-maintaining connectors. The fiber connectors are installed in the experimental setup as connectors C1 and C2 (see Figure 3.4). In case the fiber connector is not specifically stated, a PM connector is installed. The fiber connectors can be fixed onto the bench using either a simple metal clamp (not pictured) or a special L-bracket mount for the connectors (see Figure 3.8d).


(a) PM connector (b) Connector A (non-PM) (c) Connector B (non-PM) (d) L-bracket fixation for connector [18]

Fig. 3.8: Types of utilized and analyzed fiber connectors

## 3.3 Characterization of Injected Noise

This chapter describes how the acoustic and seismic noise, respectively, is injected into the FUT and presents the individual spectra of the noise.

The acoustic noise is injected into the FUT via a small speaker which is placed on the noisy bench close to the FUT. A smartphone is connected to a speaker via Bluetooth and plays the acoustic noise generated by the application named *MultiTone*. For the noise, options range between single-frequency tones, sweeps, white noise and pink noise. Pink noise is chosen since it includes more of the relevant low-frequency noise than the white noise. The spectrum of the acoustic pink noise recorded at the FUT is shown in Figure 3.9a and compared to the acoustic signal without injected noise. It is seen that the injected acoustic noise becomes noticeable for frequencies higher than 60 Hz.

The seismic noise generated by a function generator and amplifier is injected into the FUT via a seismic actuator which is tightly clamped onto the noisy bench. The options using the

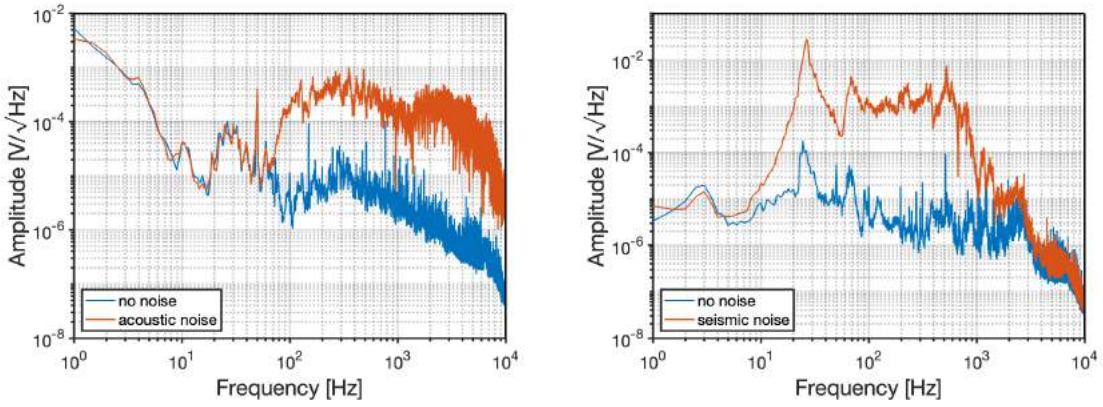


(a) pink acoustic noise (b) white seismic noise

Fig. 3.9: Spectra of injected environmental noise compared to no noise injection

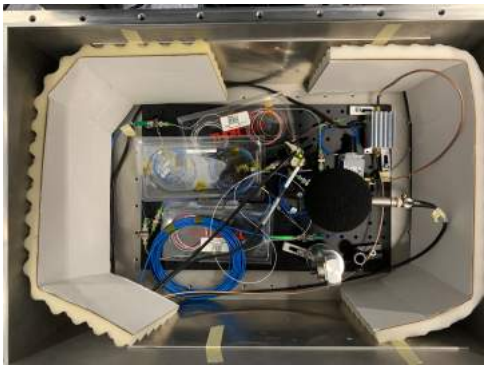

(a) reference box, inside

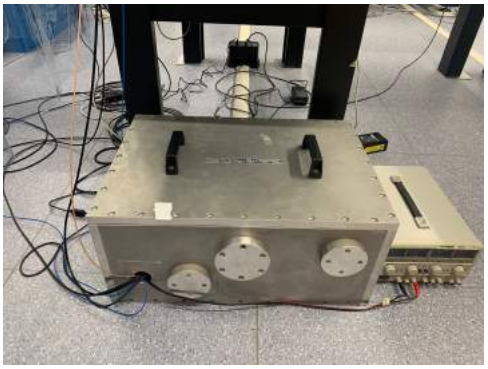

(b) reference box, outside

Fig. 3.10: Pictures of stainless steel box containing the reference

function generator are either a single-frequency signal or white noise. Here, white noise is selected for the seismic actuator since it covers a broad frequency band. In order to decide on the most suitable bandwidth of the white noise, various seismic signals of different bandwidths are recorded by the seismic sensor and compared. The bandwidth of 500 Hz yields the most suitable seismic noise, covering all the interesting low frequencies. The selected spectrum of white seismic noise is shown in Figure 3.9b and compared to the seismic signal without injected noise. It can be seen that the seismic noise is particularly noticeable for frequencies between approximately 10 Hz and 1000 Hz.

## 3.4 Characterization of Reference Box

In order to improve the isolation of the reference arm from the environmental noise injected into the FUT and consequently enhance the beating signal, a box made of stainless steel is utilized to contain most of the components of the setup. This includes everything except the FUT arm going to the noisy bench. Figure 3.4 visualizes the components placed inside the reference box as shown in the gray rectangle labeled "reference". The box consists of walls of 20 mm thickness, a removable cover plate to enable modifications of the setup, and one small opening on the side for the necessary fibers and cables entering the box, which is padded with some additional foam. A picture of the inside and outside of the reference box, respectively, is shown in Figure 3.10. On the inside, the reference box is padded with egg crate foam. The stainless steel box should reflect low frequency acoustic noise rather well, while the foam is expected to help by partially absorbing higher frequencies.

To identify how effective the reference box actually is for the acoustic isolation of the reference, a measurement is performed comparing the acoustic noise $AC_{ref}$ recorded at the reference with the acoustic noise $AC_{FUT}$ recorded at the FUT. Therefor, the pink acoustic noise displayed in Figure 3.9a is injected on the noisy bench with and without the reference box. The frequency-dependent ratio $AC_{ref}/AC_{FUT}$ is calculated for each setup

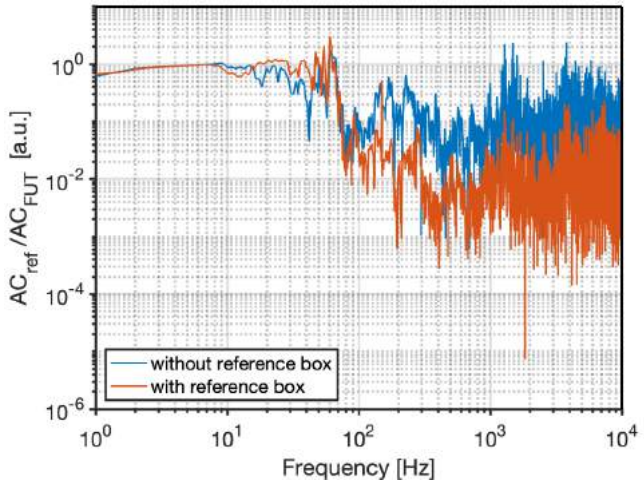


Fig. 3.11: Ratio of acoustic noise at the reference ($AC_{ref}$) to the acoustic noise at the FUT ($AC_{FUT}$) for experimental setup with and without installed reference box

and the resulting curves are shown in Figure 3.11. It is observed that the recorded ratio of acoustic noise arriving at the reference is significantly reduced when placing it inside the reference box, especially for frequencies larger than 100 Hz. Hence, employing the reference box for acoustic isolation is justified.

As for the seismic isolation, it is expected that the reference box is well-isolated from the injected seismic noise since the seismic actuator is directly fixed on the noisy bench and the reference box is placed a few meters away on the ground. However, to confirm this assumption, a measurement of the seismic noise detected at various locations is conducted. Locations include the noisy bench where the FUT is placed, the reference box and a separate table used to seismically isolate single components (such as the fiber mirror or fiber connectors) in the vicinity of the noisy bench. Since only one seismic detector is available, it is moved from one location to the next, recording the seismic signal when either no noise or white seismic noise (see Figure 3.9b) is injected on the noisy bench. The recorded signal at the reference and on the separate table is compared to the noise recorded with the seismic actuator on the noisy bench, respectively, in Figures 3.12a and 3.12b.

It is observed that generally the seismic signal recorded on the noisy bench is significantly higher than at the reference or on the separate table. Furthermore, when injecting white noise and no noise the seismic signal at the reference and on the separate table are of a similar order of magnitude. Hence, the reference box and the separate table can be considered seismically isolated from the noisy bench. However, it is noted that around the frequency of 26 Hz all seismic signals with an injected seismic white noise exhibit a maximum. This can be traced back to the maximum in the spectrum of the injected

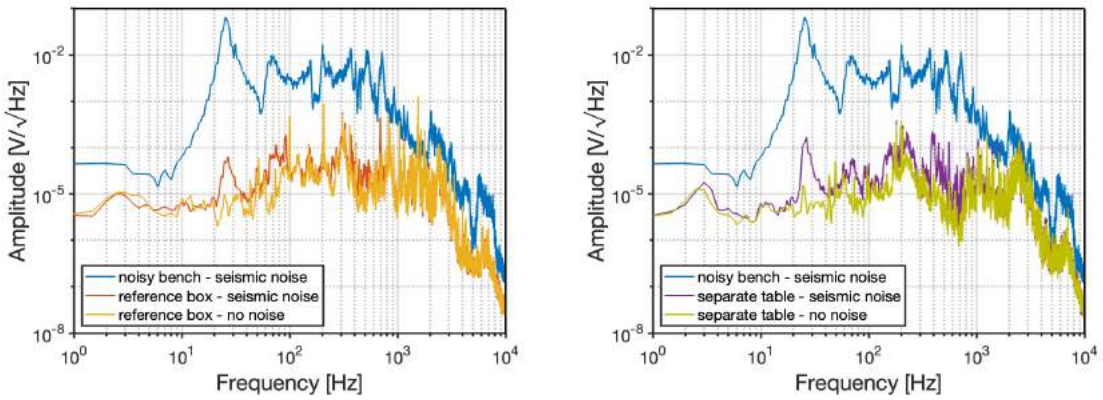


(a) seismic isolation of reference box

(b) seismic isolation of separate table

Fig. 3.12: Seismic signal recorded on the noisy bench compared to (a) the signal in the reference box and (b) the signal on the separate table, when injecting seismic noise and no noise, respectively

noise (see Figure 3.9b). Additionally, it is noticeable that the separate table is slightly less isolated than the reference box. This can be explained by the proximity of the separate table to the noisy bench.

# 4 Experiments

So far, in Chapter 2, the underlying theory for the following experiments was introduced. This included the basic concepts of optical fibers as well as the optical phase noise and its importance in gravitational wave detection. Furthermore, the beating signal representing the optical phase noise which will be recorded in the following experiments was derived mathematically. Then, the experimental setup was discussed and assembled in Chapter 3. Additionally, the optical fibers and fiber connectors which will be utilized and analyzed were introduced. Moreover, the acoustic and seismic noise which is going to be injected was presented. Finally, the acoustic and seismic isolation of the reference resulting from the installed reference box was characterized.

In this chapter, the experimental measurements will be performed and their results will be discussed. In Chapter 4.1, various optical fibers and fiber connectors will be analyzed in terms of their phase sensitivity to the injected acoustic and seismic noise, respectively. In Chapter 4.2, three different approaches to mitigate the optical phase noise induced in an optical fiber due to environmental noise will be investigated. Specifically, taping of the fiber under test to the noisy bench, placing it inside an aluminum box filled with silicone sealant, and suspending the box using a spring.

In general, the structure of the experimental setup as shown in Figure 3.4 remains unmodified. The speaker and seismic actuator, the acoustic and seismic sensors, and the reference box are not changed. The speaker and seismic sensor remain placed on the noisy bench or clamped below. The seismic sensor and one acoustic sensor are on the noisy bench, the second acoustic sensor is placed inside the reference box. The content of the reference box, which is depicted in the sketch of the setup (see Figure 3.4) in the grey box labelled "reference", is not altered. Furthermore, the electronic installation and the injected noise as previously characterized in Chapter 3.3 are unchanged throughout the experiments.

However, throughout the measurements adjustments are made on the test arm including the optical fiber under test, the connectors C1 and C2, and the fiber mirror. The FUT and/or fiber connectors are chosen from the ones introduced in Chapter 3.2. In case connectors C1 and C2 are not explicitly specified, a PM connector is utilized. Typically, the FFT of the recorded beating signal is saved. It indicates the amplitude spectral density (which will for simplicity be called "amplitude") per given frequency of the optical phase noise between 1 and 10 kHz. The FFT of the beating signal is always sampled at a frequency of 20 kHz and averaged over ten measurements. Additionally, the signal recorded with the two acoustic sensors and the seismic sensor can be read and saved.

Because the beating signal is very sensitive to environmental noise when measuring the

effect of injected acoustic and seismic noise on the induced optical phase noise, the general environmental noise additionally has a considerable influence on the signal. In the process of setting up the experiment, it has been noticed that, for example doors being shut in the building of the laboratory or people walking in the hallways significantly increase the amplitude spectral density of the induced optical phase noise across a large frequency band and thus significantly influence the result of a measurement. Subsequently, an attempt is made to use only the measurements of the beating signal which were recorded during a period of low general environmental noise.

Furthermore, the recorded beating signal and the injected environmental noise are found to be incoherent and thus not linearly dependent on each other. This is most likely a result of the vibrations of the fiber exceeding the length related to one wavelength, hence oscillating by more than $2\pi$ in phase. This phenomenon is called phase-wrapping. Consequently, generating a simple linear transfer function of the system relating the noise injection to the resulting beating signal is not conclusive and thus not reasonable. Therefore, only the absolute amplitude spectral densities of the recorded beating signal are analyzed. Due to the phase-wrapping, it is additionally assumed that the frequency of the injected environmental noise does not implicitly transfer into the optical fiber as optical phase noise of the same frequency.

Besides, the absolute values of the FFT of the beating signal are directly dependent on the laser power. However, though unmodified throughout the experiments, the laser power still appears to oscillate from time to time. Therefore, in the evaluation of the recorded signals, the relative rather than the absolute amplitudes are considered and discussed for the sake of finding the least sensitive fiber components as well as an efficient method to mitigate the induced optical phase noise.

## 4.1 Sensitivity of Fiber Components to Environmental Noise

In order to be able to mitigate the optical phase noise in the fiber components, their behavior when injected with environmental acoustic and seismic noise needs to be investigated first. Therefore, multiple measurements of the beating signal of the fibers and fiber connectors are performed to identify their sensitivity to the acoustic and seismic noise. The spectra of the injected noise were previously presented in Chapter 3.3. In Chapter 4.1.1, the sensitivity of optical fibers of different lengths and jacket size to acoustic noise is analyzed. In Chapter 4.1.2, the sensitivity of the optical fibers, fiber connectors, and their fixation to seismic noise is investigated.

### 4.1.1 Acoustic Noise Injection

In the following, the behavior of the optical phase noise as well as the sensitivity of various optical fibers under the influence of acoustic noise injection is observed. All fibers under test were previously introduced in Chapter 3.1 and the spectrum of the pink acoustic noise injected on the noisy bench is as depicted in Figure 3.9a. The FUT is exchanged after each measurement while the remaining setup is unchanged. While the 10 m black fiber and the 36 m blue fiber are furled on a spool, the other fibers are placed directly on the bench. For each fiber, the beating signal is recorded and subsequently plotted. The FFTs of the beating signals for different fiber lengths as well as with different fiber jacket thicknesses are compared in Chapters 4.1.1.1 and 4.1.1.2, respectively.

#### 4.1.1.1 Different Fiber Length

To investigate the influence of fiber length on the sensitivity of a fiber to acoustic noise with its effect on the optical phase noise, the beating FFT is recorded for fibers of different lengths. The 1 m, 10 m, and 36 m blue fiber as well as the 10 m black fiber are analyzed. The measurement results are shown in Figure 4.1a, giving the FFT of the beating signal for each fiber under test.

It can be observed that the 36 m blue fiber is the most sensitive to acoustic noise. The 1 m blue fiber, on the other hand, is the least sensitive with about two orders of magnitude less than the 36 m fiber. The two 10 m fibers (blue and black) behave rather similarly for frequencies of up to 70 Hz and above 1 kHz. For the frequencies in between, the blue fiber seems to be less sensitive to the injected acoustic noise than the black fiber. However, the fact that the 10 m black and 36 m blue fiber are on a plastic spool likely affects the measurement, either in an oscillation amplifying or damping manner. The results are generally as expected since the injected noise is assumed to have a greater influence on a longer fiber with a longer optical path length. Following from these results, the 1 m blue fiber is as of now considered the reference since it is the least affected by the injected noise and contains the same amount of fiber connections as the other fibers under test.

#### 4.1.1.2 Different Fiber Jacket

Next, the influence of the fiber's jacket thickness on its sensitivity to acoustic noise is analyzed. Therefore, the beating signal is recorded when injecting pink acoustic noise into the 1 m fiber (used as a reference), the 3 m thin fiber, and the 99:1 beam splitter. The 1 m fiber has a Ø3 mm jacket while the 3 m thin fiber and the beam splitter have a thinner Ø900 µm jacket. Figure 4.1b displays the FFT of the recorded beating signal for each fiber under test.

It can be seen that the 3 m thin fiber is the most sensitive to the injected acoustic noise,

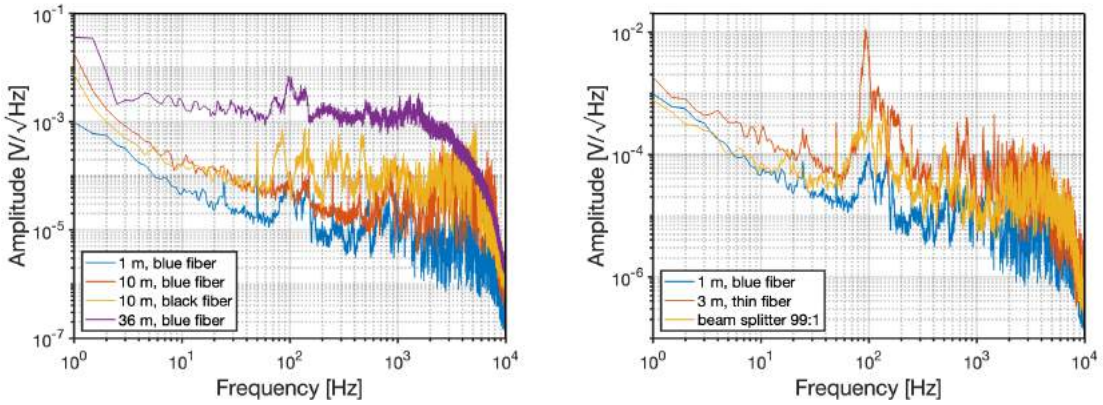


(a) different fiber lengths (b) different fiber jacket thickness

Fig. 4.1: Beating FFT of different optical fibers under acoustic noise injection

especially for frequencies around 90 Hz. The beam splitter is less sensitive to the acoustic noise than the 3 m thin fiber for frequencies up to 1 kHz and then behaves similarly for higher frequencies. Compared to the shorter 1 m fiber with a larger jacket, it is clearly noticeable that both, the 3 m thin fiber and the 99:1 beam splitter, are more sensitive to the injected acoustic noise and thus the phase noise of the laser light inside the fiber is considerably increased. Although the fibers utilized in the measurement do not have the same length, the expected tendency that thinner jackets result in an increased effect of acoustic noise on the optical phase noise can be observed. This would, however, have to be confirmed with a more scientific measurement using fibers of the same length and only varying the size of the jacket.

### 4.1.2 Seismic Noise Injection

Following the analysis of various optical fibers under acoustic noise, the effect of seismic noise injected into the fibers and connectors is investigated in terms of the induced optical phase noise. The white seismic noise with a bandwidth of 500 Hz as displayed in Figure 3.9b is injected via the seismic actuator which is fixed on the noisy bench. The sensitivity of various optical fibers (Chapter 4.1.2.1), fiber connectors (Chapter 4.1.2.2) and their fixation to the bench (Chapter 4.1.2.3) is determined by recording the individual beating signals and subsequently analyzing and comparing their FFTs.

#### 4.1.2.1 Different Optical Fibers

First, the influence of seismic noise on the optical phase noise in various optical fibers is analyzed. Fibers under test are the 1 m, 10 m, and 36 m blue fiber as well as the 10 m black fiber and the 99:1 beam splitter. All components of the FUT arm (the two PM connectors, the FUT, and the fiber mirror) are placed on the noisy bench. The two connectors are

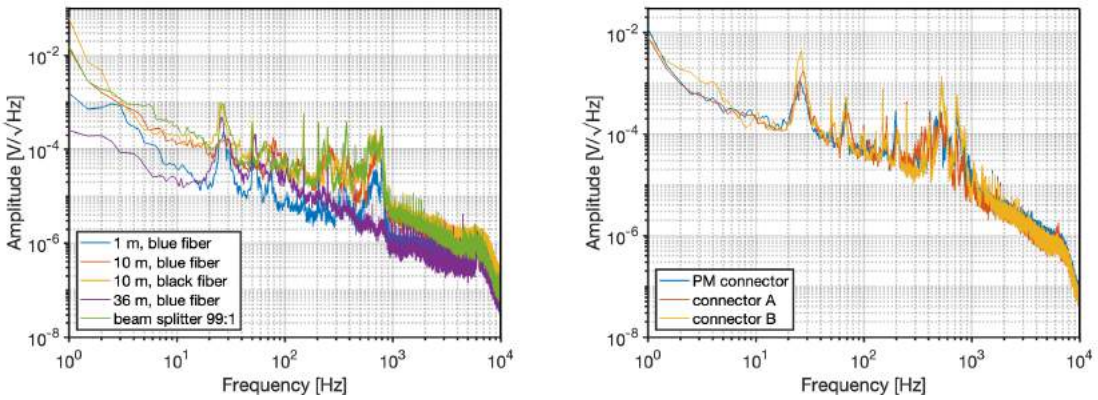


(a) different optical fibers (b) different fiber connectors

Fig. 4.2: Beating FFT of different optical components under seismic noise injection

fixed on the noisy bench such that their placement is not modified when exchanging the optical fiber. All fibers under test are loosely lying on the noisy bench, except for the 36 m fiber which is still furled on a spool for practical reasons. The measurement results of the FFTs of the beating signals for each fiber when injected with seismic noise are displayed in Figure 4.2a.

It can be observed that the two 10 m fibers and the beam splitter produce a rather similar beating signal. The beating signal of the 1 m fiber yields a comparable behavior, however, with lower magnitude since it has the shortest path, again justifying its application as the reference fiber. Furthermore, the 36 m fiber seems to be responding to the injected seismic noise in a different manner from the other fibers under test since its beating FFT does not exhibit an additional peak around 800 Hz. This response could be explained by the fact that the spool on which the 36 m fiber is wound up might attenuate the higher frequency seismic noise. Generally, the results are as expected.

#### 4.1.2.2 Different Fiber Connectors

Next, the sensitivity of the available fiber connectors to the seismic noise is examined, looking for the least sensitive and thus most suitable connector to use in the experiments on optical phase noise mitigation in Chapter 4.2. Therefore, all components of the FUT arm are placed on the separate table for seismic isolation. Only the fiber connector C1 is clamped onto the noisy bench, where the seismic noise is injected. The connectors under test are the PM connector, connector A, and connector B which were previously presented in Chapter 3.2. The 1 m blue fiber is installed as the FUT throughout the measurements, while varying the connector on the noisy bench. The resulting beating FFTs recorded for each connector under test are shown in Figure 4.2b.

It is noted that the recorded FFTs of the beating signal for each connector are very similar under seismic noise injection. The main considerable difference lies at the resonance frequency of 26 Hz, where connector B exhibits the highest peak and the PM connector the lowest. Additionally, the beating signal of connector 2 shows notably higher peaks around 530 Hz and 730 Hz than connector B and the PM connector do. Since the PM connector shows slightly lower sensitivity to the injected seismic noise, as would be expected, and because of the fact that it is the only polarization-maintaining connector and thus more mechanically precise, it will consequently be installed in all future measurements.

#### 4.1.2.3 Different Fiber Connector Fixations

After determining the PM connector as the seismically most isolated and thus most suitable connector to be installed in the experimental setup, the next task is to investigate the induced optical phase noise with different connector mountings on the noisy bench. Fixations under test are basic clamping of the fiber to the bench, an L-bracket intended for fiber connectors (see Figure 3.8d), and no fixation of the fiber connector.

For the measurements, the setup is arranged as described in Chapter 4.1.2.2. Therefor, all components of the FUT arm except for the connector under test (C1) are placed on the separate table to ensure their seismic isolation. Again, the 1 m blue fiber is installed as the FUT, while only the fixation of the connector under test is modified. The beating signal is recorded for the PM connector clamped to the noisy bench and compared to the signal of it loosely lying on the bench. The FFTs of the recorded beating signals are shown in Figure 4.3a.

It can be seen that the two signals, of the clamped and loose connector, respectively, do not differ significantly. However, the beating signal and hence the induced optical phase noise of the loose connector is slightly lower, making it the preferred choice. Possibly, the clamping with a metal clamp causes the connector to be more tightly connected to the noisy bench and thus the connector absorbs more of the injected seismic noise which in turn converts into a higher phase noise as seen in the beating signal.

Next, the optical phase noise induced when mounting the connector in the intended L-bracket fixation (see Figure 3.8d) is compared to the phase noise when the connector is loosely lying on the noisy bench. Again, the beating signal is recorded for the two configurations. The respective FFTs of the beating signals are displayed in Figure 4.3b.

It is obvious that the L-bracket connector fixation reduces the induced optical phase noise compared to the loose fiber connector. The L-bracket features better performance, mainly for frequencies between 20 Hz and 300 Hz.

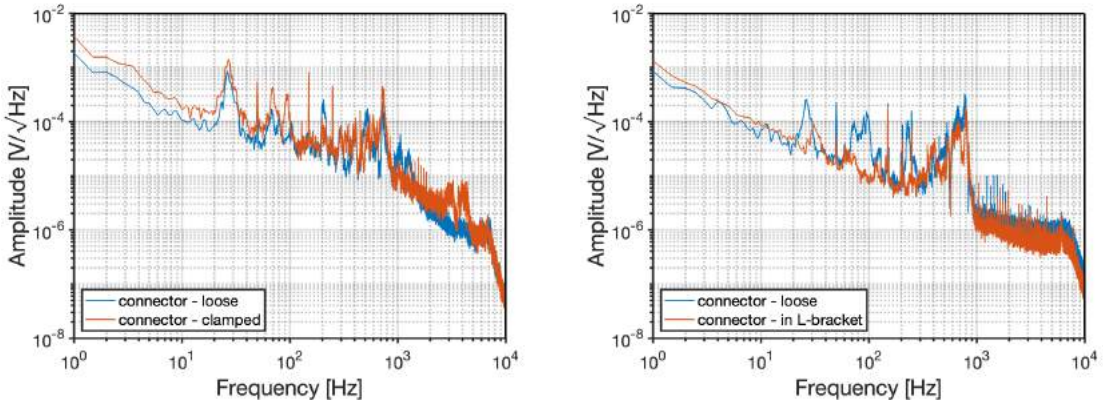


(a) PM connector either loosely lying on the noisy bench or clamped to it

(b) PM connector either loosely lying on the noisy bench or fixed onto to it with the intended L-bracket

Fig. 4.3: Beating FFT of different fiber connector fixations under seismic noise

Consequently, in order to have the least seismic noise coupling into a fiber connector as optical phase noise, the most suitable way to install connectors is by fixing them in the intended L-brackets on the bench.

## 4.2 Mitigation of Injected Environmental Noise

After analyzing the sensitivity of different optical components to environmental acoustic and seismic noise in terms of the induced optical phase noise in the previous chapter, different approaches to mitigate this noise are now tested. Therefore, three different possible methods of phase noise mitigation in the fiber under test are explored. In Chapter 4.2.1, the influence of taping the FUT to the noisy bench is investigated. In Chapter 4.2.2, the FUT is placed in a small, thick-walled aluminum box, which is additionally filled with silicone sealant and subsequently analyzed on its usefulness in mitigating the induced optical phase noise. Finally, the box containing the FUT is suspended by a spring and the resulting effect on the induced optical phase noise is analyzed in Chapter 4.2.3.

### 4.2.1 Taping of Fiber to Bench

In the following, the effect of taping the fiber under test to the noisy bench on the induced optical phase noise is analyzed. It is investigated whether taping an optical fiber to the bench increases or decreases its sensitivity and thus the induced optical phase noise when injected with acoustic and seismic noise, respectively.

For this experiment, the 10 m blue fiber (see Figure 3.6c) is utilized as the FUT since it is rather long and thus more sensitive to environmental noise than shorter fibers (as

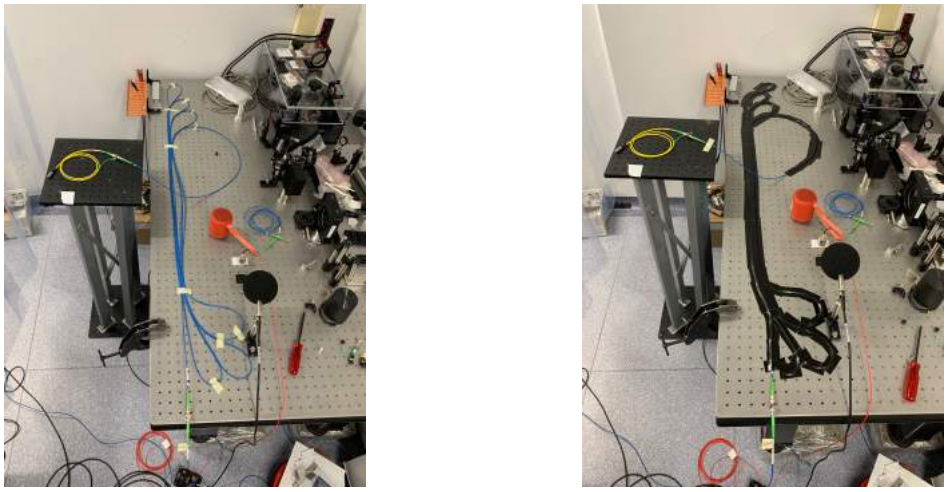

(a) fiber lying on bench, not taped (b) fiber gray taped to bench

Fig. 4.4: Pictures of 10 m blue fiber on noisy bench for taping experiment

concluded in Chapters 4.1.1.1 and 4.1.2.1), but still easy to handle compared to the 36 m option. The FUT is carefully spread out on the noisy bench using small bits of simple tape, so that the area of contact with the bench is as high as possible without tightly taping the fiber. Fiber connector C1 is placed on the noisy bench, too, while connector C2 and the fiber mirror are placed on the separate, mainly seismically isolated, table. Both connectors (C1 and C2) are polarization-maintaining. A picture of the setup without gray tape is shown in Figure 4.4a. Figure 4.4b shows a picture of the setup with the FUT taped to the noisy bench with gray tape while maintaining the remaining setup unchanged. For both configurations of the setup, with and without tape, acoustic and seismic environmental noise as characterized in Chapter 3.3 is injected on the noisy bench and hence into the FUT. The resulting beating signal is recorded for each setup with each type of noise.

The resulting FFTs of the beating signals for acoustic and seismic noise are displayed in Figure 4.5. If no additional noise is injected, it can already be observed that the beating signal experiences a notable increase in amplitude across all frequencies up to approximately 3 kHz. When injecting acoustic noise, a noticeable increase in amplitude of the beating signal of the taped optical fiber compared to the non-taped fiber is recognized for most of the recorded frequency range. For frequencies larger than 1 kHz the amplitude spectral densities converge. In case of seismic noise injection, the recorded beating signal behaves similarly. Here, the taped fiber exhibits an increased beating amplitude across all recorded frequencies compared to the non-taped fiber, too.

Consequently, taping the optical fiber to the noisy bench increases its sensitivity to environmental noise and hence the induced optical phase noise. This behavior can be explained

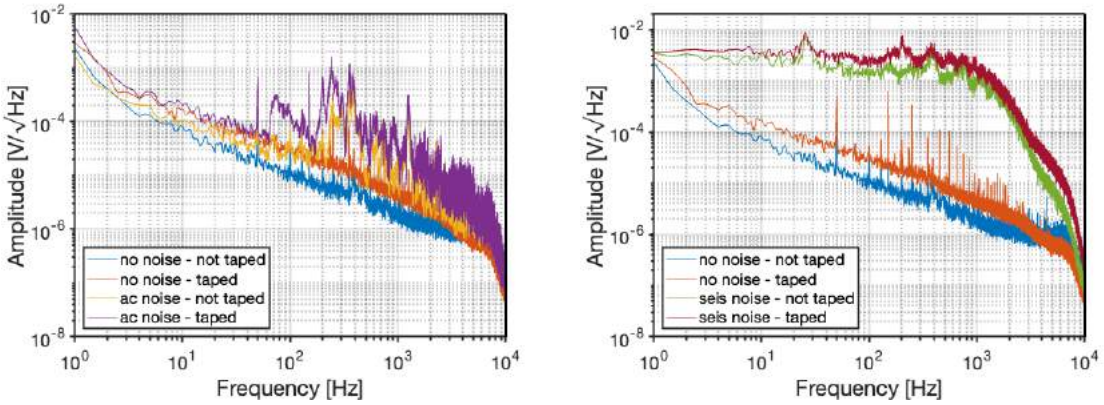


(a) acoustic noise injection (b) seismic noise injection

Fig. 4.5: Beating FFT of 10 m fiber with and without taping to noisy bench under environmental noise injection

by the enhanced connection between the FUT and the noisy bench resulting from the taping. Since the optical fiber is more tightly connected to the bench, more of the injected environmental noise is coupling into the optical fiber through the bench's surface, making it more sensitive. When not taped to the bench, the fiber is touching the noisy bench only at some places while its other parts are somewhat hovering above it. At least for the seismic noise, this can directly explain why the taping causes an increase in the induced optical phase noise. In terms of the acoustic noise, the explanation is similar. Since the acoustic noise propagates via pressure waves in the air, the initial expectation was that the taping of the fiber does not have much of an influence on the phase noise when under acoustic noise or that taping might even decrease the induced phase noise by minimizing oscillations of the fiber in the air. From the result that taping the optical fiber to the noisy bench increases the induced phase noise, however, it is concluded that the connection to the bench is indeed a significant disadvantageous aspect when analyzing for the phase noise induction. Acoustic noise is consequently coupling into the bench as seismic noise, as well, propagating through the bench. Accordingly, the injected acoustic noise is transferred to the optical fiber via acoustic and seismic noise, increasing the induced optical phase noise in the fiber as shown in Figure 4.5.

Acoustic and seismic noise are both types of mechanical noise and subsequently lead to similar effects on the phase noise. However, it is assumed that not all frequencies of acoustic noise couple into the bench to the same degree, depending on the inherent resonance frequencies of the bench and other components. Consequently, specific frequencies of seismic noise are transferred more strongly than others. A resonance frequency which can clearly be recognized in most FFTs of the recorded beating signals throughout the thesis is at 26 Hz. Furthermore, it is observed that the seismic noise injection induces a much higher

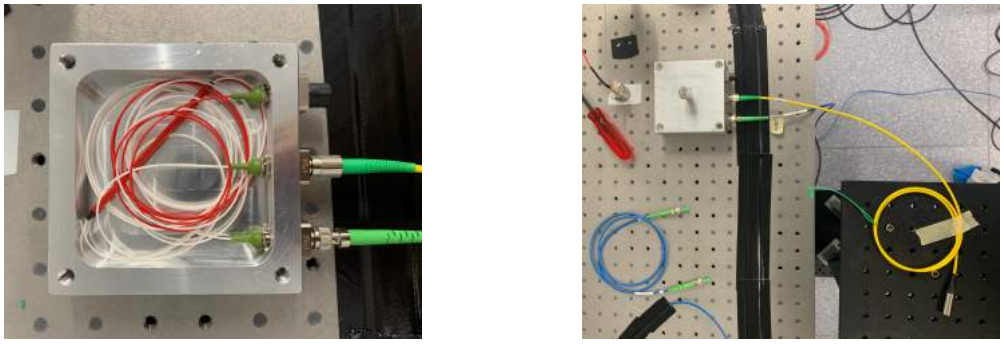

(a) open box (b) closed box

Fig. 4.6: Pictures of 99:1 beam splitter in aluminum box

optical phase noise in the optical fiber than the acoustic noise. This might be due to the stronger coupling of seismic noise in the bench, and thus the optical fiber, than in case of the acoustic noise or simply because the injected seismic noise has a higher magnitude than the acoustic noise.

### 4.2.2 Fiber in Isolated Box

Next, it is investigated whether placing an optical fiber in an aluminum box can mitigate the induced optical phase noise due to an injected environmental noise.

The 99:1 beam splitter (see Figure 3.7b) is utilized as the fiber under test, using the single-side as the input and the 99 % arm of the double-side as the output. The fiber is placed and mounted in a 10 x 10 $cm^2$ aluminum box with 1 cm wall thickness as shown in Figure 4.6a and the fiber connectors (C1 and C2) are tightly mounted in the side of the box. The aluminum box is then placed on the noisy bench and the fiber mirror on the separate table as shown in Figure 4.6b. For both acoustic and seismic noise, respectively, the beating signal is recorded for the case of the box without the lid (see Figure 4.6a) and the closed box (see Figure 4.6b). Additionally, the box is filled with a silicone sealant and then closed to analyze whether the mitigation of optical phase noise induced in the fiber is improved.

The recorded FFTs of the measured beating signals for the three box configurations with either acoustic or seismic noise injection are shown in Figure 4.7. When injected with acoustic noise, the three beating signals do not noticeably differ. For seismic noise all beating signals are very similar. However, the main peak at 26 Hz is reduced by approximately one order of magnitude when the box is filled with silicone sealant.

Consequently, the aluminum box does not provide any additional acoustic isolation to the optical fiber and is not beneficial regarding the optical phase noise mitigation induced

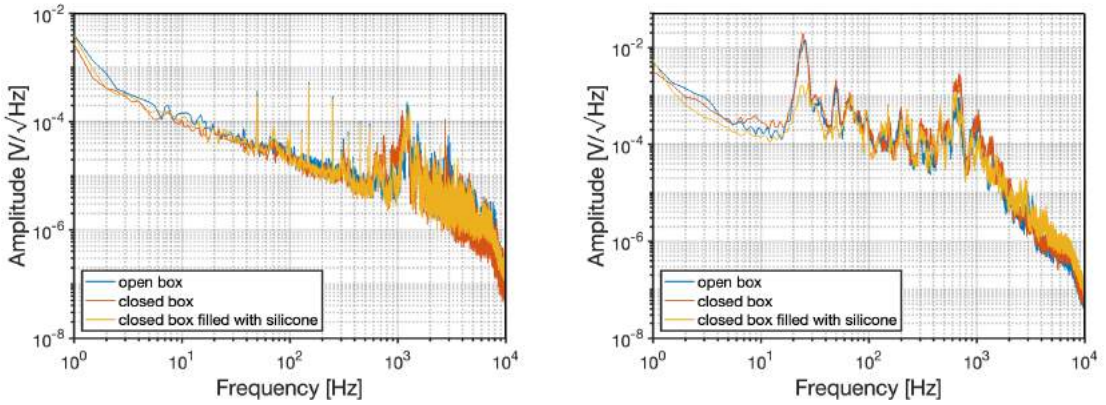


(a) acoustic noise injection (b) seismic noise injection

Fig. 4.7: Beating FFT for 99:1 beam splitter placed in an aluminum box which is either open, closed or filled with silicone sealant under environmental noise injection

by acoustic noise. Neither does the silicone sealant have any significant influence on the sensitivity of the fiber under acoustic noise. For seismic noise, enclosing the optical fiber in the aluminum box by itself does not provide isolation across the frequency range either. However, the silicon sealant significantly reduces the induced optical phase noise at the main resonance frequency of 26 Hz by one order of magnitude.

### 4.2.3 Fiber in Box Suspended by Spring

Another possibility to isolate an optical fiber and consequently mitigate the optical phase noise induced in an optical fiber by environmental noise might be the suspension of the fiber, which will be investigated in the following.

Since suspending an optical fiber can become rather tricky and inconsistent, the aluminum box from the previous Chapter 4.2.2 is utilized. The content of the box remains unchanged, still containing the 99:1 beam splitter and silicone sealant as well as adopting the previous fiber connections and the fiber mirror placement on the separate table. A spring is fixed on top of the aluminum box to enable its suspension (see Figure 4.8a). Subsequently, the box including the beam splitter can be suspended and experimental measurements can be conducted.

Since the spring constant $k$ of the spring was unknown, a simple experiment was performed to approximate $k$. The time $t$ for $n = 20$ oscillations of the spring was stopped using a stop watch. The basic spring formula giving the resonance frequency

$$f = \frac{1}{2\pi}\sqrt{\frac{k}{m}} \tag{31}$$

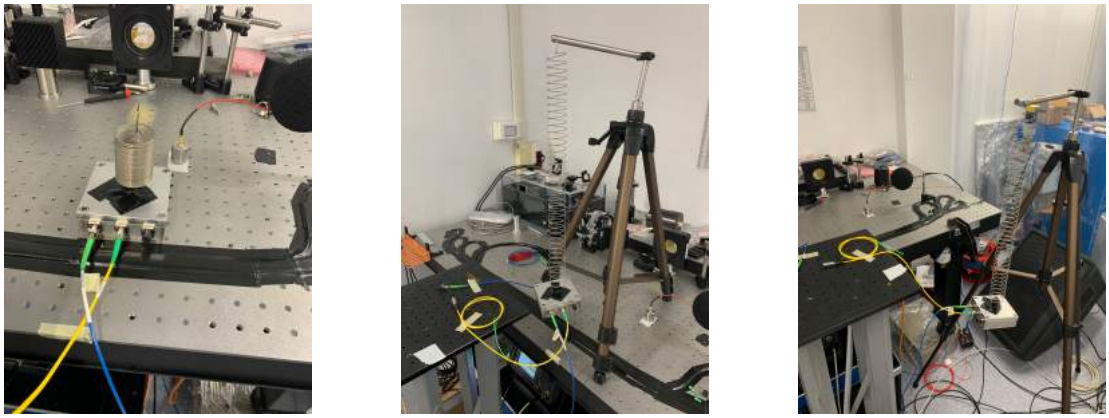

(a) box with spring placed on noisy bench

(b) box suspended on tripod standing on noisy bench

(c) box suspended on tripod standing on ground

Fig. 4.8: Picture of suspension setup with aluminum box from Chapter 4.2.2

is rearranged and with $f = \frac{n}{t}$ becomes

$$k = m\left(\frac{2\pi n}{t}\right)^2. \tag{32}$$

Inserting the utilized mass $m = 0.96$ kg and the time $t = 28.5$ s for $n = 20$ oscillations results in an approximate spring constant of $k = 18.66\frac{\mathrm{N}}{\mathrm{m}}$ for the utilized spring.

First, the influence of the suspended mass on the induced optical phase noise is studied. Therefore, the box is suspended from a simple tripod which is placed on the noisy bench where the seismic and acoustic noise is injected (see Figure 4.8b). Then, the beating signal under the environmental noise injection is recorded. Furthermore, additional masses are fixed on the box containing the optical fiber which increases the total mass of the spring system. An additional mass thus decreases the resonance frequency (see Eq. 31) and consequently lowers the cutoff frequency of the spring low pass filter. The values of the total mass suspended by the spring are stated in Table 4.1. Just like before, the beating signal is recorded with acoustic and seismic noise injection. The beating signal is then compared to the signal recorded for the unsuspended box placed on the noisy bench (see Figure 4.8a). The FFTs of the recorded beating signals under acoustic and seismic noise are displayed in Figures 4.9a and 4.10a, respectively.

Table 4.1: Total masses of aluminum box containing the FUT suspended by spring

| **label** | **mass $m$** |
|---|---|
| suspension | 960 g |
| suspension - mass 1 | 1309 g |
| suspension - mass 2 | 1700 g |

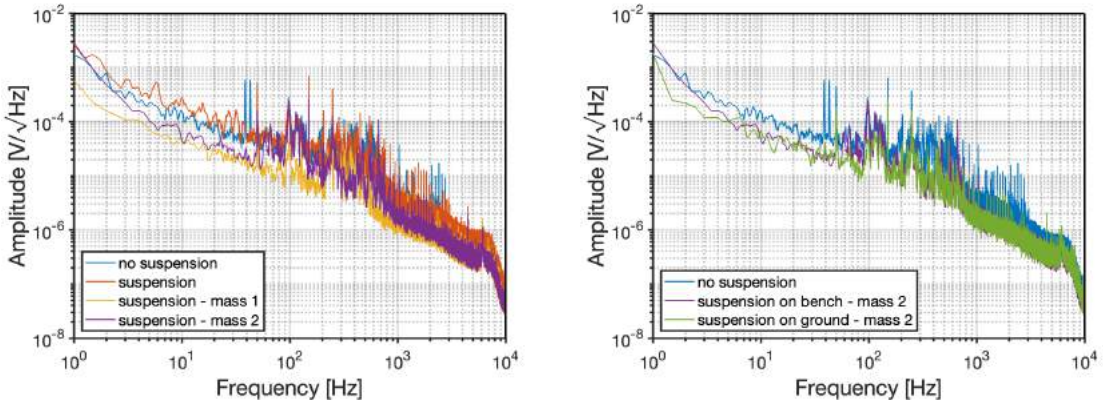


(a) influence of suspended mass on optical phase noise

(b) comparison of beating FFT when suspended on noisy bench and ground

Fig. 4.9: Beating FFT of fiber in box suspended by spring under acoustic noise injection

Next, the induced optical phase noise with the highest mass suspended from the tripod placed on the noisy bench is compared to the noise when the tripod with the spring is placed on the ground. A picture of this setup is shown in Figure 4.8c. The FFTs of the recorded beating signals under acoustic and seismic noise are displayed in Figure 4.9.

The FFTs of the recorded beating signals under acoustic noise as shown in Figure 4.9 exhibit rather small differences between the different measurements. In Figure 4.9a, the results for no suspension and the suspension without an additional mass do not differ considerably. The results for the suspension with additional masses 1 and 2 are slightly lower. However, this seems more like a systematic offset since it is not frequency-specific. This might have been caused by a random decrease in laser power or a decrease in general environmental noise during the period of measurement.

When comparing the recorded optical phase noise induced in the FUT for the tripod standing on the noisy bench with the tripod standing on the ground (see Figure 4.9b), the FFTs of the beating signals are very similar. The only significant difference is noticed for frequencies between approximately 60 and 200 Hz, where the beating signal with the suspension on the ground is slightly lower. This result matches previous results as well as expectations. Since acoustic noise propagates through air via pressure differences, the location of the box containing the FUT, as long as the configuration is the same, is not very crucial. The placement of the tripod is solely important for the part of the acoustic noise which couples into matter, here either the noisy bench or the ground, as seismic noise. However, since the spring system does not produce a significant difference in the beating signal, the seismic noise resulting from the acoustic noise is comparably small.

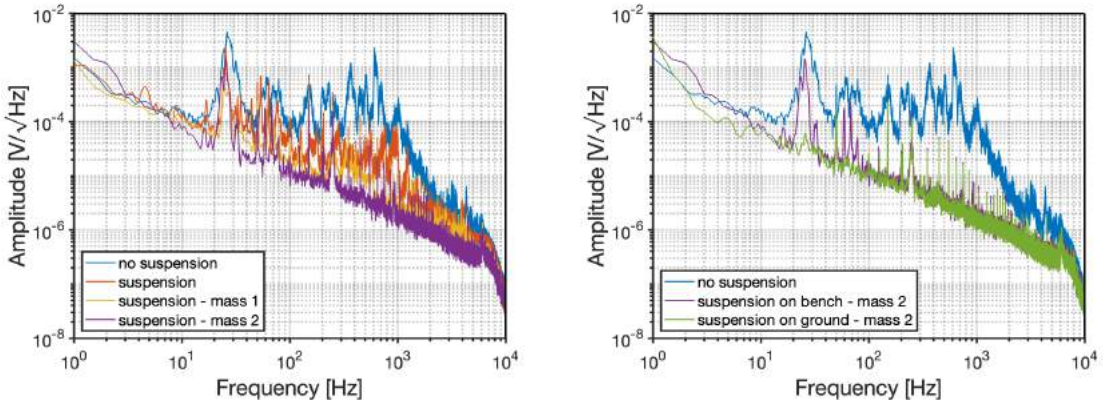


(a) influence of suspended mass on optical phase noise

(b) comparison of beating FFT when suspended on noisy bench and ground

Fig. 4.10: Beating FFT of fiber in box suspended by spring under seismic noise injection

Overall, for acoustic environmental noise it can be concluded that the suspension of an optical fiber does not significantly mitigate the induced optical phase noise and hence does not offer considerable acoustic isolation of the fiber.

Looking at the recorded FFTs of the beating signals under seismic noise injection, which are shown in Figure 4.10, the resulting signals exhibit significant differences. In Figure 4.10a, it can be seen that the setup configuration with the FUT placed on the noisy bench without a suspension leads to the highest amplitude. The amplitude then decreases across all frequencies with increasing mass of the spring system containing the FUT. Subsequently, the optical phase noise induced in the optical fiber due to seismic noise can be significantly decreased by installing a spring suspension system. Thereby, a higher mass on the spring suspending the optical fiber leads to increased seismic isolation and thus lower optical phase noise.

Moreover, for increased masses the amplitude of the beating signal and thus of the optical phase noise even converges with the amplitude of the beating in the setup on the ground which is expected to be seismically well-isolated (see Figure 4.10b). An exception is found around the main resonance frequency of 26 Hz, for which the suspension provides only a marginal improvement.

Consequently, the suspension of an optical fiber using a spring system is an effective method to mitigate the induced optical phase noise in a fiber due to seismic noise.

# 5 Conclusion

In this thesis, the influence of environmental acoustic and seismic noise on the optical phase noise induced in optical fibers was analyzed and different approaches to mitigate this noise were investigated.

The experimental setup of a heterodyne interferometer with a well-isolated reference arm was assembled in Chapter 3, based on the underlying theory of the optical phase noise and the recorded beating signal as discussed in Chapter 2. Then, the behavior of the induced optical phase noise in various optical components under environmental noise injection was analyzed in Chapter 4.1. Therefore, the sensitivity of optical fibers to acoustic noise was first investigated in terms of the induced optical phase noise. The assumption that longer fibers and thinner fiber jackets lead to an increased sensitivity to the injected noise was confirmed. Next, the sensitivity of optical fibers and fiber connectors to seismic noise was analyzed with regard to the induced optical phase noise. Similarly to the acoustic noise, the shorter optical fiber exhibits lower optical phase noise and hence is less sensitive to seismic noise. Moreover, the fiber with a thinner jacket is much more sensitive to seismic noise. When taking a look at the fiber connectors, no significant difference is seen in the measurements results. However, the fixation of the connector to the bench seems to be of importance since the L-bracket fixation yields the lowest optical phase noise. After gaining knowledge about the behavior of optical fibers and their sensitivity to acoustic and seismic noise injection, three potential ways of mitigating the induced optical phase noise were examined in Chapter 4.2. Taping of the fiber under test to the bench was found to increase the induced optical phase noise caused by acoustic and seismic noise and is hence unfavorable for the fiber's sensitivity. When isolating the fiber in an aluminum box filled with a silicone sealant, it was found that the sensitivity at the resonance frequency can be decreased mainly for seismic noise. Subsequently, the box containing the fiber was suspended by a spring. From the recorded beating signal was concluded that the suspension is the most useful method to mitigate the induced optical phase noise. Especially for seismic noise injection in the spring system, the optical fiber exhibits much lower amplitudes in the FFT of the beating signal, and thus a lower optical phase noise. Furthermore, it is observed that a higher mass suspended on the spring leads to a decreased sensitivity of the optical fiber.

The results obtained from the performed experiments confirm previous assumptions on the fiber sensitivity and hint at a possible direction for optical phase noise mitigation induced in optical fibers due to environmental noise. Possible suspension systems for the optical fiber to minimize the induced optical phase noise are without a doubt worth further investigations. Additionally, a suitable gel to embed the optical fiber in and minimize the effect of a specific frequency range of environmental noise is worth an investigation.

# References


[1] RP Photonics. *Phase Noise*. URL: https://www.rp-photonics.com/phase_noise.html (visited on 26. 09. 2022).

[2] Eugene Hecht. *Optik*. 7th ed. Berlin Boston : De Gruyter, 2018. ISBN: 9783110526653.

[3] Andreas Müller. *10 Dinge, die Sie über Gravitationswellen wissen wollen. Von schwächsten Signalen und stärksten Ereignissen*. Springer-Verlag Berlin Heidelberg, 2017. ISBN: 978-3-662-54408-2. DOI: 10.1007/978-3-662-54409-9.

[4] B. P. Abbott et al. "Observation of Gravitational Waves from a Binary Black Hole Merger". In: *Physical Review Letters* 116 (6 02/2016), p. 061102. DOI: 10.1103/PhysRevLett.116.061102.

[5] Barry C. Barish. "Nobel Lecture: LIGO and gravitational waves II". In: *Rev. Mod. Phys.* 90 (4 12/2018), p. 040502. DOI: 10.1103/RevModPhys.90.040502.

[6] Matthieu Gosselin. *Theory of Setup and Beating Signal*. Internal communication. 05. 04. 2022.

[7] Matthieu Gosselin. *Mathematical Derivation of Beating Signal*. Internal communication. 01. 07. 2022.

[8] Matthieu Gosselin. "High Power fibered optical components for Gravitational Waves detectors". PhD thesis. University of Pisa, 2018.

[9] Govind P. Agrawal. *Fiber-Optic Communication Systems*. 4th ed. Wiley-Interscience, 2010. ISBN: 9780470918517.

[10] Michael Bass. *Handbook of Optics, Vol. 2: Devices, Measurements, and Properties*. 2nd ed. McGraw-Hill Professional, 1995. ISBN: 9780070479746.

[11] Akis P. Gatzoulis and Dennis R. Pape. *Design and Fabrication of Acousto-optic Devices*. Marcel Dekker, 1994. ISBN: 9780824789305.

[12] RP Photonics. *Schematic setup of acousto-optic modulator*. URL: https://www.rp-photonics.com/img/aom.webp (visited on 24. 09. 2022).

[13] Thorlabs. *P3-1064PM-FC-1 - PM Patch Cable, PANDA, 1064 nm, Ø3 mm Jacket, FC/APC, 1 m*. URL: https://www.thorlabs.com/thorproduct.cfm?partnumber=P3-1064PM-FC-1 (visited on 02. 10. 2022).

[14] Thorlabs. *P3-1064PM-FC-2 - PM Patch Cable, PANDA, 1064 nm, Ø3 mm Jacket, FC/APC, 2 m*. URL: https://www.thorlabs.com/thorproduct.cfm?partnumber=P3-1064PM-FC-2 (visited on 02. 10. 2022).

[15] Thorlabs. *P3-1064PM-FC-10 - PM Patch Cable, PANDA, 1064 nm, Ø3 mm Jacket, FC/APC, 10 m*. URL: https://www.thorlabs.com/thorproduct.cfm?partnumber=P3-1064PM-FC-10 (visited on 02. 10. 2022).

[16] Thorlabs. *P3-780PMY-2 - PM Patch Cable, PANDA, 780 nm, Ø900 µm Jacket, FC/APC, 2 m*. URL: https://www.thorlabs.com/thorproduct.cfm?partnumber=P3-780PMY-2 (visited on 02. 10. 2022).

[17] Thorlabs. *PN1064R1A1 - 1x2 PM Coupler, 1064 ± 15 nm, 99:1 Split, ≥20 dB / ≥16 dB PER, FC/APC Connectors*. URL: https://www.thorlabs.com/thorproduct.cfm?partnumber=PN1064R1A1 (visited on 02. 10. 2022).

[18] Thorlabs. *ADABS1 - Single L-Bracket for Square Flange FC Mating Sleeves*. URL: https://www.thorlabs.com/thorproduct.cfm?partnumber=ADABS1 (visited on 02. 10. 2022).

## Eidesstattliche Erklärung

Hiermit versichere ich an Eides statt, dass ich diese Arbeit selbstständig verfasst und keine anderen als die angegebenen Quellen und Hilfsmittel benutzt habe. Außerdem versichere ich, dass ich die allgemeinen Prinzipien wissenschaftlicher Arbeit und Veröffentlichung, wie sie in den Leitlinien guter wissenschaftlicher Praxis der Carl von Ossietzky Universität Oldenburg festgelegt sind, befolgt habe.

Oldenburg, den

| 12.11.2022 | B. v. Boetticher |
| --- | --- |
| Datum | Unterschrift |